



# A facile strategy of enhancing interaction between cerium and manganese oxides for catalytic removal of gaseous organic contaminants

Jin Chen<sup>a</sup>, Xi Chen<sup>a,b</sup>, Dongxu Yan<sup>a,b</sup>, Mingzhu Jiang<sup>a,b</sup>, Wenjian Xu<sup>a</sup>, Hao Yu<sup>c</sup>, Hongpeng Jia<sup>a,c,\*</sup>

<sup>a</sup> CAS Center for Excellence in Regional Atmospheric Environment, Institute of Urban Environment, and Key Laboratory of Urban Pollutant Conversion, Institute of Urban Environment, Chinese Academy of Sciences, Xiamen, 361021, China

<sup>b</sup> University of Chinese Academy of Sciences, Beijing, 100049, China

<sup>c</sup> College of Chemical and Environmental Engineering, Shandong University of Science and Technology, Qingdao, 266590, China



## ARTICLE INFO

### Keywords:

Redox etching-precipitation  
VOCs  
Catalytic oxidation  
Manganese oxide  
Cerium oxide

## ABSTRACT

A facile strategy of redox etching-precipitation is developed to support cerium oxide ( $\text{CeO}_3$ ) on crystal  $\alpha$ -type manganese dioxide nanorod (OMS). By means of this method, the contact between  $\text{CeO}_3$  and OMS can be strengthened and results in enhancement of interfacial effect, thereby causing consequent changes in physicochemical properties. Through screening and evaluation, the as-prepared catalyst of 5.0%  $\text{CeO}_3/\text{OMS}$  (5.0% Ce/OMS) with an optimal Ce/Mn molar ratio of 0.05, owning more acidity, more superficial oxygen vacancies as well as more mobility of lattice oxygen, exhibits a remarkable activity and stability for catalytic oxidation of chlorobenzene. Under catalysis of 5.0% Ce/OMS, the demanded temperature for complete removal of chlorobenzene is about 360 °C, which is lower than the required temperature (above 400 °C) for  $\text{NH}_3\text{-}5.0\%$  Ce/OMS prepared via conventional method of  $\text{NH}_3\text{-H}_2\text{O}$  precipitation. Meanwhile, 5.0% Ce/OMS shows a good tolerance to high water content (10 vol.%) and a better recyclability, adapts to oxidation of various kinds of volatile organic compounds (VOCs) and VOCs mixture under simulated realistic exhaust condition. With correlation of structure and performance, it is revealed that interface acts as active site to catalyze oxidation.

## 1. Introduction

Volatile organic compounds (VOCs) as a group of gaseous contaminations have damage to the environment and human health [1]. Hence, the emission of VOCs is limited by more and more strict legislation, which makes more attention paid on development of efficient controlling technologies. Catalytic oxidation is considered as the most promising approach to diminish emission of high-concentration VOCs from manufacture, due to less secondary pollution and energy input [2–4]. The catalysts, playing a key role to determine efficiency of catalytic oxidation, are usually classified into noble metals and transition metal oxides [5,6]. Although the noble metal catalysts own higher activity, the transition metal oxides have advantages in terms of cost and stability. Therefore, much attempt has been made in developing new methods to obtain transition metal catalysts with high activity and stability as substitutes for noble metal catalysts [5,7,8].

Manganese oxide is a choice of alternative transition metal oxides for removal of gaseous pollutants [9–12]. Nevertheless, its performance cannot satisfy practice demands, for instance, in terms of stability at

severe condition and low-temperature activity to some kinds of VOCs, ascribed to instinct natures of individual metal oxides. To improve physicochemical properties, the formation of mixed metal oxides (MMO) by introducing hybrid metals (e.g. Cu, Ag, Fe, Ce) is popularly implemented [13,14]. The facilitation is mainly ascribed to the influence of interfacial effect between different oxides on physicochemical natures [15–18]. The conventional methods such as impregnation, alkaline precipitation and co-precipitation are commonly used to prepare MMO [19,20]. With progress of synthetic technology, the application of combustion method and redox precipitation in synthesis of MMO has been recently reported [16,21]. For instance, the cerium and manganese mixed oxides ( $\text{Ce}-\text{MnO}_x$ ) prepared by either combustion method or redox precipitation can exhibit remarkable activity to catalyze oxidation of VOCs such as toluene and *o*-xylene [16,21–23]. We have ever reported the hydrolysis-driving redox co-precipitation to synthesize homogeneous Mn-X solid solutions (X = Fe, Ce) [24,25]. The obtained catalysts are effective to remove almost aromatic VOCs, but it is also found that the activity to chlorinated VOCs (CVOCs) is poor and a great amount of active sites lost in bulk cannot participate in the reaction.

\* Corresponding author at: CAS Center for Excellence in Regional Atmospheric Environment, and Key Laboratory of Urban Pollutant Conversion, Institute of Urban Environment, Chinese Academy of Sciences, Xiamen, 361021, China.

E-mail address: [hpjia@iue.ac.cn](mailto:hpjia@iue.ac.cn) (H. Jia).

Recently, we had reported application of a novel redox etching-precipitation in successfully supporting single atom Au on manganese dioxide nanorod (OMS), so the highly-efficient utilization of precious metal was realized [40]. Because the strong interaction between Au and support facilitates the redox property of catalysts, the performance in low-temperature catalytic oxidation was promoted. In this work, the strategy is developed for the first application in synthesis of supported transition metal oxides. OMS nanorod is chosen to support cerium oxide ( $\text{CeO}_y$ ) by surface redox reaction. The surface of OMS nanorod is chemically etched by  $\text{H}_2\text{O}_2$ , meanwhile, the consumption of protons ( $\text{H}^+$ ) by the redox reaction drives hydrolysis of  $\text{Ce}^{3+}$  salt. Because of synchronous occurrence of redox and hydrolysis reactions,  $\text{Ce}(\text{OH})_3$  nanoparticles grow on the surface of OMS and then turn to  $\text{CeO}_y$  through calcination. Compared to individual metal oxides, the as-prepared catalysts ( $x\%$  Ce/OMS) perform better activities for catalyze oxidation of chlorobenzene as a kind of chlorinated VOCs (CVOCs) with high toxicity and refractory degradation. Moreover, the  $x\%$  Ce/OMS exhibits a remarkable long-term stability, tolerance to water and adaptability to various VOCs at severe reaction conditions. In fact, many reports have recently pointed out the catalytic performance of Ce-based and Mn-based oxides in combustion of CVOCs can be improved by introducing heteroatoms, as summarized in Table 1.

## 2. Experiment section

### 2.1. Chemicals and materials

The reagents with A.R. grade were used directly. Potassium permanganate ( $\text{KMnO}_4$ ), cerium (III) nitrate hexahydrate ( $\text{Ce}(\text{NO}_3)_3 \cdot 6\text{H}_2\text{O}$ ), manganese (II) sulfate monohydrate ( $\text{MnSO}_4 \cdot \text{H}_2\text{O}$ ), hydrogen peroxide ( $\text{H}_2\text{O}_2$ , 30 wt.-%), and chlorobenzene, benzene, toluene and *o*-xylene were purchased from Sinopharm Chemical Reagent Co., Ltd. (Shanghai, China).

### 2.2. Preparation

The manganese dioxide nanorod with  $\alpha$ -type structure (OMS) was synthesized by classic method [41,42]. In prior of redox etching-precipitation, a certain amount of  $\text{Ce}(\text{NO}_3)_3 \cdot 6\text{H}_2\text{O}$  was dissolved in 200 mL deionized water, and then about 2 g amount of OMS powder was redispersed ultrasonically in  $\text{Ce}(\text{NO}_3)_3$  solution. Three equivalents of stoichiometric amount of  $\text{H}_2\text{O}_2$  were diluted by 50 mL deionized water. For instance, 0.30 g of  $\text{H}_2\text{O}_2$  (30 wt%) was demanded to completely deposit 0.25 g of  $\text{Ce}(\text{NO}_3)_3 \cdot 6\text{H}_2\text{O}$  on 2.08 g of OMS, resulting in Ce/Mn molar ratio of 0.025. The  $\text{H}_2\text{O}_2$  solution was added dropwise with vigorous stirring at room temperature without controlling pH value. After filtering, washing and drying at 120 °C for 12 h, the solids were calcined at 400 °C for 4 h in air atmosphere in furnace. According to

molecule mass (86.9 g/mol) of nominal  $\text{MnO}_2$  formula, the molar ratios between Ce and Mn cations (Ce/Mn) were calculated. The obtained catalysts were donated on basis of Ce/Mn molar ratio, for example, the nominal Ce/Mn molar ratio for 2.5% Ce/OMS catalyst was 0.025. The method of  $\text{NH}_3 \cdot \text{H}_2\text{O}$  precipitation was adopted to synthesize catalysts for control experiment. Pure cerium dioxide ( $\text{CeO}_2$ ) and  $\text{NH}_3 \cdot 5.0\%$  Ce/OMS were prepared by using  $\text{NH}_3 \cdot \text{H}_2\text{O}$  instead of  $\text{H}_2\text{O}_2$  to precipitate  $\text{Ce}^{3+}$  cations, and the other procedures were the same to redox etching-precipitation.

### 2.3. Characterization

Powder X-ray diffraction (XRD) measurements were performed on PANalytical X'pert Pro instrument with X-ray irradiation source of  $\text{Cu-K}\alpha$ . The  $2\theta$  angle was scanned at the range between 10° and 90°. Transmission electronic microscopy (TEM) images were given by JEM-2100 F, H-7650 or JEOL-TEM transmission electronic microscopies. Binding energies (B.E.) and element composition in superficial layer were determined by Thermo Scientific ESCALAB 250 X-ray photoelectron spectroscopy instrument (XPS).  $\text{N}_2$  static adsorption-desorption characterization was carried out on Autosorb IQ instrument of Quantachrome Company. Brunauer-Emmett-Teller method (BET) and Barrett-Joyner-Halenda method (BJH) were utilized to calculate specific surface areas ( $S_{\text{BET}}$ ) and average pore diameter ( $D_{\text{BJH}}$ ), respectively. The metal ingredients were measured by inductively coupled plasma-optical emission spectroscopy (ICP-OES). The middle products in effluent gas were identified by on-line TC-D200 M mass spectroscopy (MS). The temperature programmed reduction/desorption characterizations ( $\text{H}_2\text{-TPR}$ ,  $\text{O}_2\text{-TPD}$ ,  $\text{NH}_3\text{-TPD}$ ) and measurement of surface oxygen vacancy concentration were carried out on chemisorption instrument (Quantachrome, Chemstar) equipped with TCD and on-line MS. *In-situ* diffuse reflection infrared Fourier transition spectroscopy (*in-situ* DRIFTS) of pyridine adsorption was performed on Thermo Scientific IS 50 equipped with Harrick reaction cell to identify acid types (Lewis/Brønsted acids). The procedures for chemisorption characterizations and *in-situ* DRIFTS are described in detail in Appendix A. Supplementary data. The calculated consumption of oxygen during measuring oxygen vacancy concentration is defined as oxygen storage capacity (OSC) [43].

### 2.4. Activity test

The catalytic performance was tested on fixed bed. The inner diameter and length of quartz tube are 6.0 mm and 410 mm, respectively. In prior of activity test, the catalyst was screened by sieves (40–60 mesh). Loading amount of catalyst was fixed at 66.6 mg, and the length of reaction layer was controlled at 2–2.5 cm. As a result, the possibilities of transfer barriers including internal and external transfer

**Table 1**

A little summary of published works about Mn-based and Ce-based oxides for catalytic oxidation of CVOCs.

Catalyst	Kind of CVOCs	Reaction conditions	Temperature at maximal conversion	Ref.
$\text{MnO}_x/\text{CeO}_2\text{-NC}$	Chlorobenzene	5000 ppm 20% $\text{O}_2/\text{N}_2$ , 20,000 $\text{h}^{-1}$	≈ 90% (400 °C)	[26]
$\text{CeMn-(0.21)-HT-N6A4}$	Trichloroethylene	1000 ppm, Air, 15,000 $\text{h}^{-1}$	100% (120 °C)	[27]
$\text{Mn-Ce-O}/\gamma\text{-Al}_2\text{O}_3$	Chlorobenzene	1000 ppm, Air, 15,000 mL/(g h)	100% (338 °C)	[28]
$\text{MnO}_x\text{-CeO}_2$ (0.86)	Chlorobenzene	1000 ppm, 10% $\text{O}_2/\text{N}_2$ , 30,000 $\text{h}^{-1}$	100% (400 °C)	[29]
$\text{MnO}_x\text{-CeO}_2$ (0.86)	Chlorobenzene	1000 ppm, 10% $\text{O}_2/\text{N}_2$ , 15,000 $\text{h}^{-1}$	100% (250 °C)	[30]
$\text{Mn}_8\text{Co}_1\text{Ce}_1$ /cordierite	Chlorobenzene	1000 ppm, 15,000 $\text{h}^{-1}$	90% (325 °C)	[31]
$\text{Ce/TiO}_2$ ( $\text{Ce}/\text{Ti} = 14$ )	1,2-Dichloroethane	1000 ppm, Air, 15,000 $\text{h}^{-1}$	90% (275 °C)	[32]
$4\text{Ce1Cr-(NH}_4)_2\text{CO}_3$	$\text{C}_2\text{H}_2\text{Cl}_2$ , $\text{C}_2\text{HCl}_3$ , $\text{C}_2\text{H}_4\text{Cl}_2$ , $\text{C}_6\text{H}_5\text{Cl}$	1000 ppm, Air, 9000 mL/(g h)	90% (222–295 °C)	[33]
$\text{PO}_x\text{-CeO}_2\text{-0.2}$	$\text{CH}_3\text{Cl}_2$	500 ppm, Air, 15,000 mL/(g h)	95% (300 °C)	[34]
$\text{Mn}_{0.8}\text{Ce}_{0.2}\text{O}_2/\text{HZSM-5}$	Chlorobenzene	1000 ppm, 10% $\text{O}_2/\text{N}_2$ , 10 vol.% $\text{H}_2\text{O}$ , 15,000 mL/(g h)	90% (250 °C)	[35]
5Fe-CeO <sub>2</sub> -ST	1,2-Dichloroethane	250 ppm, Air, 15,000 mL/(g h)	90% (237 °C)	[36]
$\text{La}_3\text{Mn}_2\text{O}_7\text{-P}$	Dichloromethane	0.1 vol.% DCM, 10% $\text{O}_2/\text{N}_2$ , 15,000 mL/(g h)	90% (380 °C)	[37]
$\text{MnCuO}_x/\text{TiO}_2$	Chlorobenzene	500 ppm, Air, 5000 $\text{h}^{-1}$	100% (350 °C)	[38]
$\text{Mn}_2\text{O}_3/\gamma\text{-Al}_2\text{O}_3$	Dichloroethane	100 ppm, 20.8% $\text{O}_2$ , 80000 $\text{h}^{-1}$	95% (700 K)	[39]

limitations are avoided via adjusting reaction conditions. Reaction temperature was monitored at the bottom of catalyst layer by K-type thermocouple. The air stream containing a certain concentration of VOCs and 0–10 vol.% content of water vapor passed through catalyst layer with flow rate of 66.6 mL/min, giving a weight hourly space velocity (WHSV) of 60,000 mL/(g h). Considering the practice application in the VOCs control, the combined technologies such as adsorption-condensation (by zeolite rotor or activated carbon) and catalytic oxidation are widely used for purification of the exhaust from manufactory. The concentration of VOCs is usually elevated by the adsorption-condensation process before catalytic oxidation. Therefore, to simulate real conditions, the catalytic experiments were carried out by using concentration at between 500 ppm and 1000 ppm. To investigate the influence of reaction condition, the reaction parameters (WHSV, concentration and humidity) were adjusted. The composition in outlet gas was analyzed by the on-line GC equipped with a FID and a TCD. The VOCs conversion ( $X_{VOC}$ ) and total conversion ( $X_{Total}$ ) of VOCs mixture were calculated on basis of difference in VOCs concentration, and the mineralization ( $Y_{CO_2}$ ) was estimated according to the change of  $CO_2$  concentration. The concentration of  $CO_2$  in outlet gas ( $c(CO_2)_{outlet}$ ) increased with elevated temperature until VOCs was completely oxidized into  $CO_2$  at a certain temperature.  $CO_2$  concentration ( $c(CO_2)_{Complete}$ ) was constant even when the temperature was further increased to higher temperature than that for complete mineralization. The relevant calculation was carried out by using these equations as below:

$$X_{VOC} = \frac{c(VOC)_{outlet}}{c(VOC)_{inlet}} \times 100\%$$

$$X_{Total} = \frac{\sum X_{VOC} \times c(VOC)}{\sum c(VOC)}$$

$$Y_{CO_2} = \frac{c(CO_2)_{outlet}}{c(CO_2)_{Complete}} \times 100\%$$

Notably, no CO could be detected by TCD and some by-products that can not be determined by FID were identified by on-line MS.

### 3. Results and discussion

#### 3.1. Illustration of strategy

An important target in preparation of MMO is to enhance interfacial effect by strengthening interaction between different metal oxides, which is believed to be favourable to the improvement of catalytic performance [44–46]. We herein show a chemical route to “plant”  $CeO_y$  nanoparticles on the surface of OMS. As we know, the reversible hydrolysis of transition metal salts in aqueous solution releases  $H^+$  ions like this:  $Ce^{3+} + 3H_2O \rightleftharpoons Ce(OH)_3 + 3H^+$  ( $K_{sp}^0([Ce^{3+}] [OH^-]^3) = 1.5 \times 10^{-20}$ ). The hydrolysis proceeds forward by consumption of  $H^+$  ions. In fact,  $H^+$  ions could be consumed by a redox reaction between  $MnO_2$  species and  $H_2O_2$  as follows:  $MnO_2(s) + H_2O_2(l) + 2H^+(aq) \rightleftharpoons Mn^{2+}(aq) + 2H_2O(l) + O_2(g)$  ( $\Delta G = -102.1 \text{ kJ/mol}$ ). Therefore, the combination of hydrolysis and redox reaction leads to a spontaneous reaction as follows:  $3MnO_2(s) + 3H_2O_2(l) + 2Ce^{3+}(aq) \rightleftharpoons 3Mn^{2+}(aq) + 2Ce(OH)_3(s) + 3O_2(g)$  ( $\Delta G = -80.1 \text{ kJ/mol}$ ). The  $Mn^{4+}$  ions on the surface of OMS are reduced to soluble  $Mn^{2+}$  ions, so the site is chemically etched. Given synchronism of redox and hydrolysis reactions,  $Ce(OH)_3$  nanoparticles could be firmly planted on OMS as illustrated by Scheme 1 and were further treated to form  $x\% Ce/OMS$ .

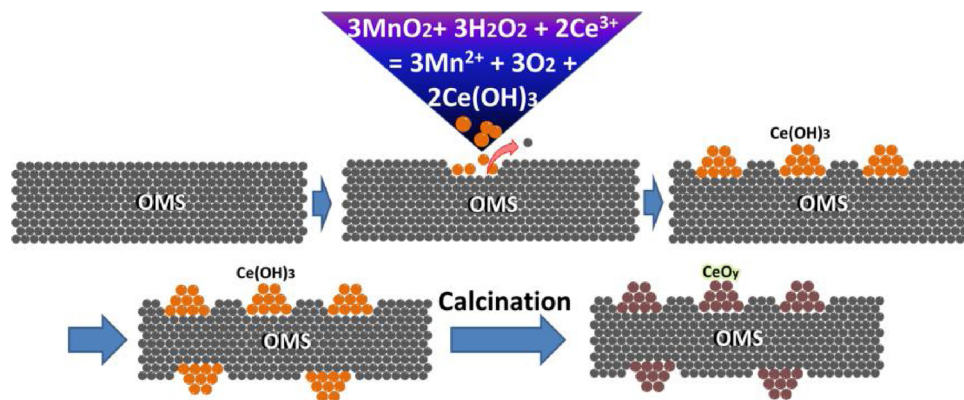
#### 3.2. Characterization

For validation of the feasibility in supporting  $CeO_y$  on OMS via redox etching-precipitation, ICP-OES is applied to distinguish difference

in element composition. The measured Ce/Mn molar ratios by ICP-OES in Table 2 are actually close to nominal values. The composition in superficial layer is probed by XPS. According to XPS spectra and peak areas (Fig. S1 and Table S1), the Ce/Mn molar ratios of surface are calculated by using relevant factors [49]. Something interesting is found that the calculated results from XPS (Table 2) are obviously higher than the nominal values and the results from ICP-OES. It implies the supported  $CeO_y$  mainly exists on the surface of OMS. When the nominal value is more than 7.5%, the Ce/Mn molar ratios based on XPS are tend to be unchanging (around 0.2), which indicates coverage of  $CeO_y$  are closely saturated. XRD patterns of all the samples are presented in Fig. 1. XRD patterns show typical diffraction peaks of  $\alpha-MnO_2$  (PDF # 00-006–0547) without any obvious diffraction peaks corresponding to  $CeO_2$  (PDF # 00-001–0800), which means  $CeO_y$  nanoparticles are highly dispersed.  $N_2$  static absorption-desorption is applied to distinguish changes of surficial structure (Fig. S2). Through calculation by means of BET and BJH methods, the values of  $S_{BET}$  and  $D_{BJH}$  are obtained. As summarized in Table 2, the variation of  $D_{BJH}$  is in fact negligible, but the gradually increasing values of  $S_{BET}$  with increased Ce/Mn molar ratios implies enlargement of the exposed surface, owing to the formation of  $CeO_y$  by chemically etching redox. In comparison to metal oxides such as 5.0% Ce/OMS ( $S_{BET} = 55 \text{ m}^2/\text{g}$ ) prepared via redox etching-precipitation,  $NH_3$ -5.0% Ce/OMS prepared via  $NH_3$ - $H_2O$  precipitation has a less  $S_{BET}$  ( $46 \text{ m}^2/\text{g}$  as shown in Fig. S5) that is close to that of OMS ( $47 \text{ m}^2/\text{g}$ ). This confirms the advantage of our synthetic strategy in enlargement of exposed surface, which is usually accompanied with formation of more surface defects. In general, the more defects are believed to provide more active sites for catalytic reaction.

The elaborative discrepancies in nanostructure is observed by TEM characterizations. As depicted in Fig. 2(a), OMS grows along the orientation of [001] axis with smooth surface. Take 5.0% Ce/OMS as an example. In Fig. 2(b), numerous  $CeO_y$  nanoparticles are laid on nanorod. Because of higher atomic number of Ce than Mn,  $CeO_y$  nanoparticles look brighter at dark field of HAADF-STEM in Fig. 2(c). In HRTEM of Fig. 2(d), the lattice fringes with 0.349 nm and 0.312–0.315 nm distances are assigned to lattice planes of  $\alpha-MnO_2$  {220} and  $CeO_2$  {111}, respectively. Meanwhile, the smooth surface of OMS turns to rough, due to appearance of more holes, and  $CeO_y$  particles are trapped in the holes. The appearance of holes on OMS surface is ascribed to  $H_2O_2$  chemical etching. The width of  $CeO_y$  nanoparticles along the specific orientation is measured. As depicted in Fig. 2(e), the mean width (4.40 nm) along z axis paralleled with surface of OMS is longer than the one (2.34 nm) along x axis. It suggests  $CeO_y$  nanoparticles are probably hemispheric. This structure is believed to enlarge interface between  $CeO_y$  and OMS, thereby causing enhancement of interfacial effect. From seeing element distribution in Fig. 2(f–i), Ce species is homogeneously supported on OMS without any aggregation. The similar morphology is also found for  $x\% Ce/OMS$  with the other Ce/Mn molar ratios, which is displayed in Fig. S3. But aggregation of  $CeO_y$  particles occurs when Ce/Mn molar ratio increases above 7.5%. Different to 5.0% Ce/OMS, the  $CeO_y$  particles in  $NH_3$ -5.0% Ce/OMS are shaped as sphere with mean size of 4.17 nm.

As mentioned above, the nanostructure built by redox etching-precipitation is believed to enhance the Mn-Ce interaction. The effect of strong interaction on chemical natures is investigated by the following *in-situ* DRIFTS of pyridine adsorption and chemical absorption-desorption characterizations. Firstly, *in-situ* DRIFTS results pronounce variation of acidic species that is induced by supporting  $CeO_y$ . As shown in Fig. 3, the characteristic peaks maximized at  $1447 \text{ cm}^{-1}$ ,  $1457 \text{ cm}^{-1}$  and  $1540 \text{ cm}^{-1}$  belong to physical adsorption of pyridine, chemical adsorption of pyridine on Brønsted (B) and Lewis (L) acidic sites, respectively [35,50]. The relative intensity ratio between Lewis and Brønsted acid ( $I_L/I_B$ ) for 5.0% Ce/OMS (0.51) is remarkably higher than that for OMS (0.19), which means promotion effect of introduced Ce on formation of Lewis acidic site and is favorable to activate CVOCs [35]. Then, the change of acid strength is determined by  $NH_3$ -TPD. Because



**Scheme 1.** The illustration of redox etching-precipitation method to prepare x% Ce/OMS.

**Table 2**

Physicochemical properties of the catalysts.

Catalyst	Ce/Mn molar ratio		$S_{\text{BET}}$ ( $\text{m}^2/\text{g}$ )	$D_{\text{BJH}}$ (nm)	$\text{Mn}^{3+}/\text{Mn}_{\text{All}}$	$\text{Ce}^{3+}/\text{Ce}^{4+}$	$\text{O}_{\text{Latt}}/\text{O}_{\text{Ads}}$
	ICP	XPS <sup>a</sup>					
OMS	–	–	47	19	0.46	–	4.4
2.5% Ce/OMS	0.024	0.110	50	19	0.46	0.53	5.5
5.0% Ce/OMS	0.045	0.128	55	20	0.47	0.56	5.9
7.5% Ce/OMS	0.068	0.202	58	19	0.47	0.56	5.5
10.0% Ce/OMS	0.110	0.222	63	18	0.46	0.55	5.2

<sup>a</sup> Although the accuracy for element analysis from XPS is limited by some deviation [47,48], the results are still competent to distinguish the difference by measuring on the same device.

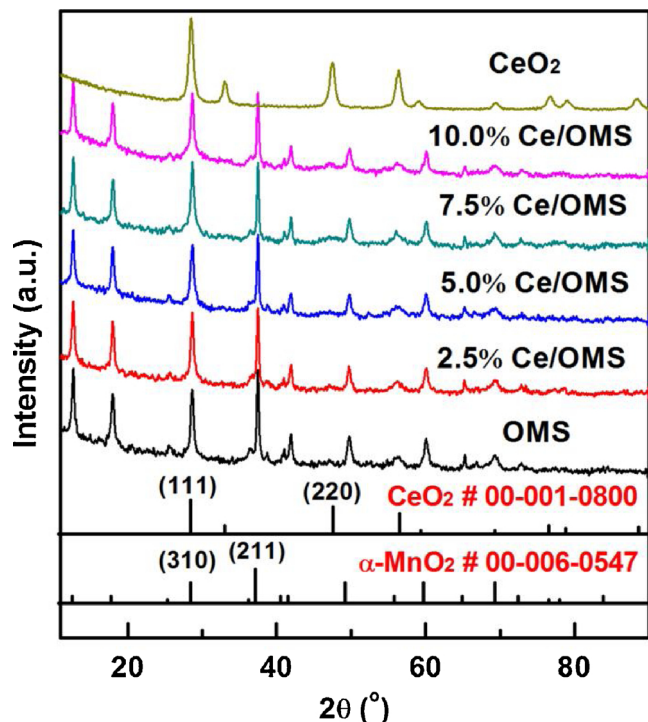


**Fig. 1.** XRD patterns of metal oxides.

desorption of oxygen and water causes interference to TCD signals (Fig. S4), MS signal of  $m/z = 17$  is adopted to NH<sub>3</sub>-TPD. As depicted in Fig. 4(a), the individual OMS owns a broad peak at low temperature (below 300 °C) and a shoulder peak at high temperature (between 300 °C and 600 °C) corresponding to NH<sub>3</sub> desorption from weak acid and strong acid, respectively [51,52]. Compared to OMS, these peaks for 2.5% and 5.0% Ce/OMS appear at higher temperature, as a symbol

for increased acid intensity. Meanwhile, the more obvious shoulder peaks are observed, which indicate more content of strongly acidic sites. Nevertheless, with further increasing of Ce/Mn molar ratio (7.5% and 10.0%), desorption temperature of all peaks shifts to lower temperature, which means a negative effect from excessive addition of Ce on acidity. The total amount of acidic sites is measured according to amount of desorbed NH<sub>3</sub> from NH<sub>3</sub>-TPD. As shown in Table 3, the most amount of NH<sub>3</sub> desorption is achieved by 5.0% Ce/OMS. It is generally thought more acidic sites and intensity are preferable to catalytic activation of hydrocarbons besides VOCs [32,52,53].

The influence on redox property is reflected on H<sub>2</sub>-TPR in Fig. 4(b). The amount of total H<sub>2</sub> consumption in Table 3 decreases gently with increased Ce/Mn molar ratio. In fact, the H<sub>2</sub> amount for total reduction of CeO<sub>2</sub> has ever been determined as 1265 μmol/g in our previous work [25], which is much less than those for reduction of obtained Mn-based metal oxides. Theoretically, only 4.7 wt.% content of oxygen takes part in reduction of CeO<sub>2</sub> to Ce<sub>2</sub>O<sub>3</sub> thereby consuming 2938 μmol H<sub>2</sub> per unit gram of CeO<sub>2</sub>, but the weight content for reduction of MnO<sub>2</sub> to MnO is 18.4 wt.% leading to 11,500 μmol/g amount of H<sub>2</sub> consumption. Meanwhile, allowing for rather proportion of Ce<sup>3+</sup> cations within CeO<sub>2</sub> sample as evidenced by XPS, it is understood that much more H<sub>2</sub> is consumed by reduction of Mn-based oxides than CeO<sub>2</sub>. Consequently, the increased content of Ce/O<sub>x</sub> must reduce amount of H<sub>2</sub> consumption for reduction of Ce/OMS oxides. As shown in Fig. 4(b), there is a broad peak for H<sub>2</sub>-TPR of OMS, which indicates multistep reduction of MnO<sub>2</sub> to Mn<sub>2</sub>O<sub>3</sub> and then to MnO, respectively [17,22]. For H<sub>2</sub>-TPR of CeO<sub>2</sub>, the peaks at low temperature (350–550 °C) are ascribed to the reduction of surface Ce<sup>4+</sup> to Ce<sup>3+</sup>, the peak at high temperature (833 °C) is probably assigned to further reduction of bulk Ce<sup>4+</sup> to Ce<sup>3+</sup> [13]. Supporting CeO<sub>y</sub> on OMS results in the slight shift to higher temperature for reduction peaks compared to pure OMS, which is probably contributed by the strong interaction between CeO<sub>y</sub> and OMS and inhibited reduction reaction between OMS and H<sub>2</sub> by CeO<sub>y</sub> covered on the surface of OMS. The reduction peaks for CeO<sub>y</sub> in H<sub>2</sub>-TPR of x% Ce/OMS cannot be obviously observed, ascribed to small amount of H<sub>2</sub>

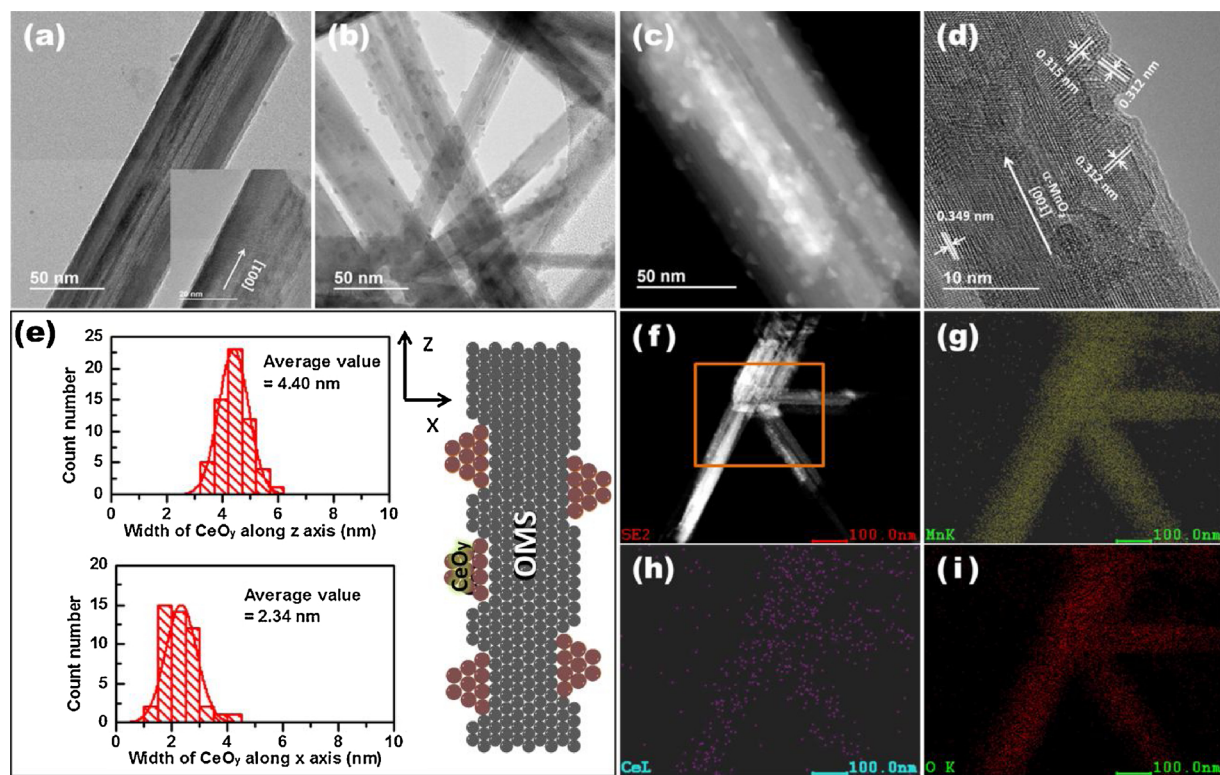


**Fig. 2.** TEM, HRTEM and HAADF-STEM images of OMS and 5.0% Ce/OMS, (a) TEM image of OMS, (b-d) TEM, HAADF-STEM and HRTEM images of 5.0% Ce/OMS, (e) size distribution of CeO<sub>y</sub> particles within 5.0% Ce/OMS along specific orientations and 2D diagram, (f-i) HAADF-STEM image and EDS mapping of Mn, Ce, O elements of 5.0% Ce/OMS.

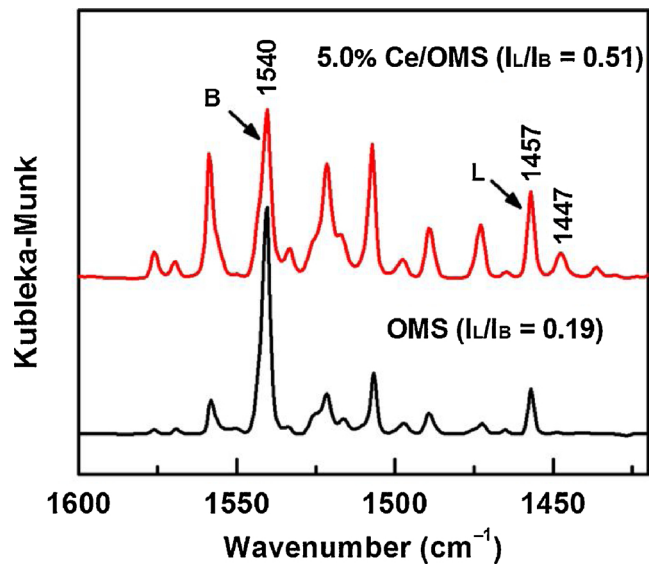


**Fig. 3.** *In-situ* DRIFTS spectra of pyridine adsorption.

consumption by CeO<sub>2</sub> reduction.

To our knowledge, catalytic oxidation of hydrocarbons commonly obeys Mars-van-Krevelen (MvK) mechanism where oxygen species of catalyst participate in the reaction, so the concentration of surface oxygen vacancy and oxygen mobility in metal oxides are considered [7,54]. The measured values of OSC listed in Table 3 demonstrate the formation of oxygen vacancy is facilitated by supporting CeO<sub>y</sub> on OMS. Hence, OSC value increases from 35 μmol/g for OMS to 201 μmol/g for 5.0% Ce/OMS, but it is not further raised when the Ce/Mn molar ratio is more than 0.05. The total amount of oxygen desorption is calculated on basis of O<sub>2</sub>-TPD in Fig. 4(c). Although only a few amount of oxygen

is desorbed from CeO<sub>2</sub> (477 μmol/g at 50–900 °C) [25], the appropriate addition of CeO<sub>y</sub> can accelerate oxygen mobility of OMS. Among them, the most amount of oxygen is desorbed from 5.0% Ce/OMS (3024 μmol/g). In Fig. 4(d), the four peaks for OMS at 116 °C, 217 °C, 474 °C and 545 °C are belonging to physisorbed molecular oxygen (O<sub>phy</sub>), surface chemisorbed oxygen (O<sub>surf</sub>), oxygen in surface lattice (O<sub>Latt</sub>), and oxygen in lattice near to the surface (O'<sub>Latt</sub>), respectively [55]. When Ce species is deposited on OMS via redox etching-precipitation, none of obvious change happens to the temperature for desorption of O<sub>phy</sub> and O<sub>surf</sub>, but the temperatures for desorption of O<sub>Latt</sub> and O'<sub>Latt</sub> are modified by tuning Ce/Mn molar ratio. Among them, the species of O<sub>Latt</sub> and O'<sub>Latt</sub> within 5.0% Ce/OMS and 2.5% Ce/OMS are easily emitted, so the temperatures for desorption are lowest (471 °C and 525 °C). In the other word, the appropriate Ce/Mn molar ratio is favorable to the activation of lattice oxygen.

XPS as a powerful tool to study natures of surface is carried out. In Fig. 5(a), the spectra of O-1 s are divided into three peaks. The peaks centered at around binding energy (B.E.) of 532.3–532.4 eV, 531.2–531.3 eV and 529.7 eV belong to the hydroxyl/adsorbed-water oxygen (O<sub>(-OH)</sub>), the adsorbed oxygen (O<sub>ads</sub>) and the surface lattice oxygen (O<sub>Latt</sub>), respectively [27,30]. According to the peak areas, the ratios between O<sub>Latt</sub> and O<sub>ads</sub> are calculated. As shown in Table 2, O<sub>Latt</sub>/O<sub>ads</sub> ratio undergoes an increasing tendency initially with increasing of Ce/Mn molar ratio, but the excess addition of Ce leads to reducing of O<sub>Latt</sub>/O<sub>ads</sub> ratio. Among them, the highest value of O<sub>Latt</sub>/O<sub>ads</sub> ratio (5.9) is realized by 5.0% Ce/OMS. This indicates appropriate amount of CeO<sub>y</sub> addition is beneficial for mobility of the lattice oxygen from bulk to surface, which is agreed by O<sub>2</sub>-TPD. Given the coordination of oxygen and metal ions, the variation of O<sub>Latt</sub>/O<sub>ads</sub> ratio is actually related to the valence change of metallic cations on the surface. To distinguish the differences, the broad peak of Mn-2p<sub>3/2</sub> (B.E. = 642.2 eV) in Fig. 5(b) is fitted into three peaks at 641.0 eV, 642.2 eV and 643.7 eV belonging to Mn<sup>2+</sup>, Mn<sup>3+</sup> and Mn<sup>4+</sup> ions [56], meanwhile, the peaks of Ce-3d in

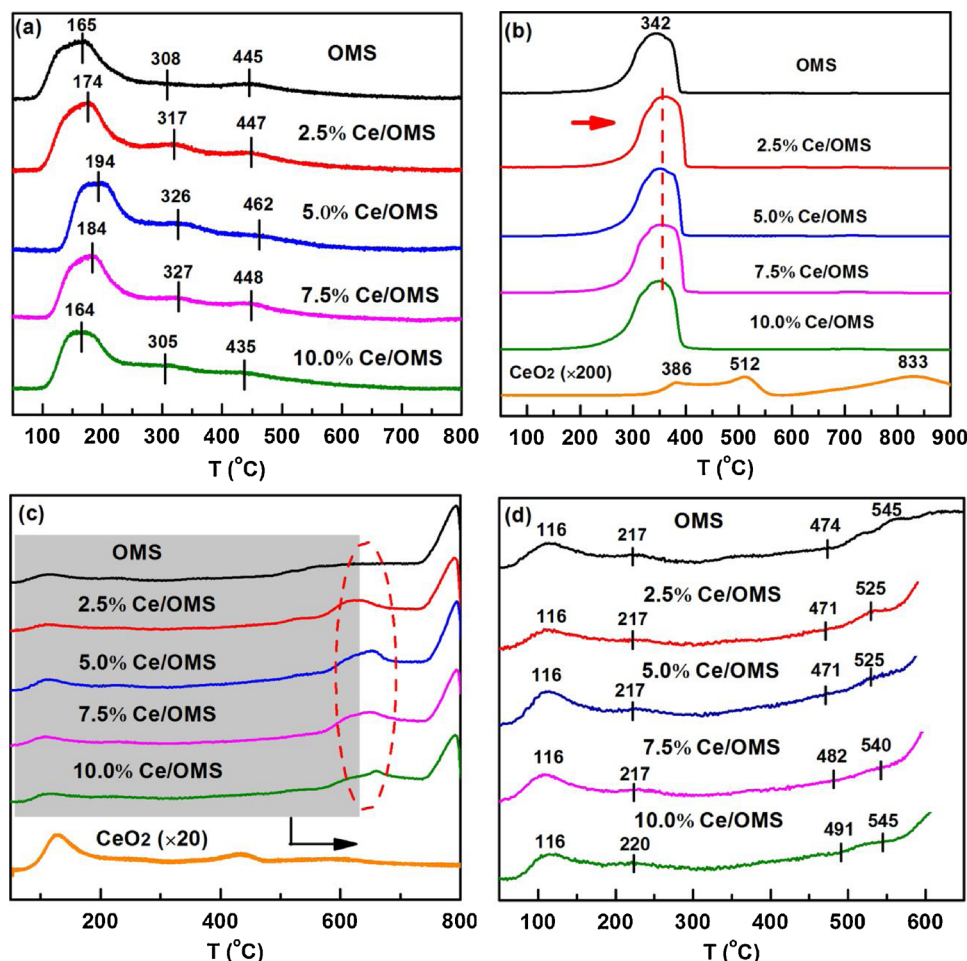


**Fig. 4.** Temperature-programmed desorption/reduction spectra of various catalysts, (a) NH<sub>3</sub>-TPD, (b) H<sub>2</sub>-TPR, (c) O<sub>2</sub>-TPD at full range, and (d) O<sub>2</sub>-TPD at temperature range between 50 °C and 650 °C.

**Table 3**  
Chemical properties of the as-prepared catalysts.

Catalyst	NH <sub>3</sub> -TPD (μmol/g)	H <sub>2</sub> -TPR	O <sub>2</sub> -TPD	OSC <sup>a</sup>
OMS	394	11501	2728	35
2.5% Ce/OMS	471	11565	2929	147
5.0% Ce/OMS	530	10716	3024	201
7.5% Ce/OMS	478	10858	2735	194
10.0% Ce/OMS	445	10460	2716	197

<sup>a</sup> OSC is oxygen storage capacity calculated according to amount of consumed O<sub>2</sub> during titration.

**Fig. 5(c)** are fitted into multiple peaks corresponding to Ce<sup>3+</sup> and Ce<sup>4+</sup> ions according to literatures [13,57]. Generally, the cations of Mn<sup>3+</sup> and Ce<sup>3+</sup> are thought to be related to formation of lattice oxygen, because the reversible valence changes of cations (Mn<sup>3+</sup> ⇌ Mn<sup>4+</sup> + e and Ce<sup>3+</sup> ⇌ Ce<sup>4+</sup> + e) donates some electrons to activate oxygen during catalytic reaction [56,58]. On basis of peak areas, the relative content of different-valence cations is calculated. As shown in **Table 2**, the proportion of Mn<sup>3+</sup> is improved by introducing appropriate amount of CeO<sub>y</sub>, but the change is very slight. However, it can be observed that Ce<sup>3+</sup>/Ce<sup>4+</sup> ratio changes with increasing of Ce/Mn molar ratio, where 5.0% Ce/OMS and 7.5% Ce/OMS obtain the highest ratio of 0.56. In the other word, Ce/Mn molar ratio has a direct influence on relative content of Ce<sup>3+</sup> ions which is related to activation and mobility of lattice oxygen.

From another viewpoint, the influence of valence change on

physicochemical properties is also explained. Du et al. have recently pointed out the heterogeneous junction existing in Ce-Mn mixed oxides is the key to modification of physicochemical properties [13]. Namely, there is strong interaction between Ce and Mn oxides. The different valence states of Mn and Ce cations are readily recognized by XPS. Among them, Ce<sup>3+</sup> and Mn<sup>4+</sup> cations mainly exist at states of Ce<sub>2</sub>O<sub>3</sub> and MnO<sub>2</sub>. According to literature, the conduction band energies (E<sub>c</sub>) vs standard hydrogen electrode for Ce<sub>2</sub>O<sub>3</sub> and MnO<sub>2</sub> are −0.5 eV and 1.33 eV correspondingly [59]. Hence, MnO<sub>2</sub> with more positive E<sub>c</sub> is approached to get electrons from Ce<sub>2</sub>O<sub>3</sub> at interface, thereby leading to a lack of electrons within Ce<sub>2</sub>O<sub>3</sub>. Nevertheless, the electrophilicity of Ce<sub>2</sub>O<sub>3</sub> is improved to strengthen (Lewis) acidity as evidenced by *in-situ* DRIFTS and NH<sub>3</sub>-TPD. Meanwhile, the lattice oxygen of OMS could be activated by Ce cations through the Zener exchange owing to reversible electron transfer between Ce<sup>3+</sup> and Mn<sup>4+</sup>, so more content and more mobility of lattice oxygen within Ce-Mn binary oxides are found by XPS and O<sub>2</sub>-TPD [15,60]. Therefore, the physicochemical properties are varied by tuning interfacial effect via changing Ce/Mn molar ratio.

### 3.3. Catalytic performance

By considering its high toxicity and difficult degradation, chlorobenzene is chosen as model pollutant to test capacity for catalytic oxidation of VOCs. The performance is firstly evaluated under the conditions of 1000 ppm chlorobenzene, WHSV of 60,000 mL/(g h) and 5 vol.% of water vapor. In fact, catalytic reaction commonly consists of multiple stages from activation of substrate to desorption of products [24,25]. The conversion is just abatement of VOCs in feed gas which

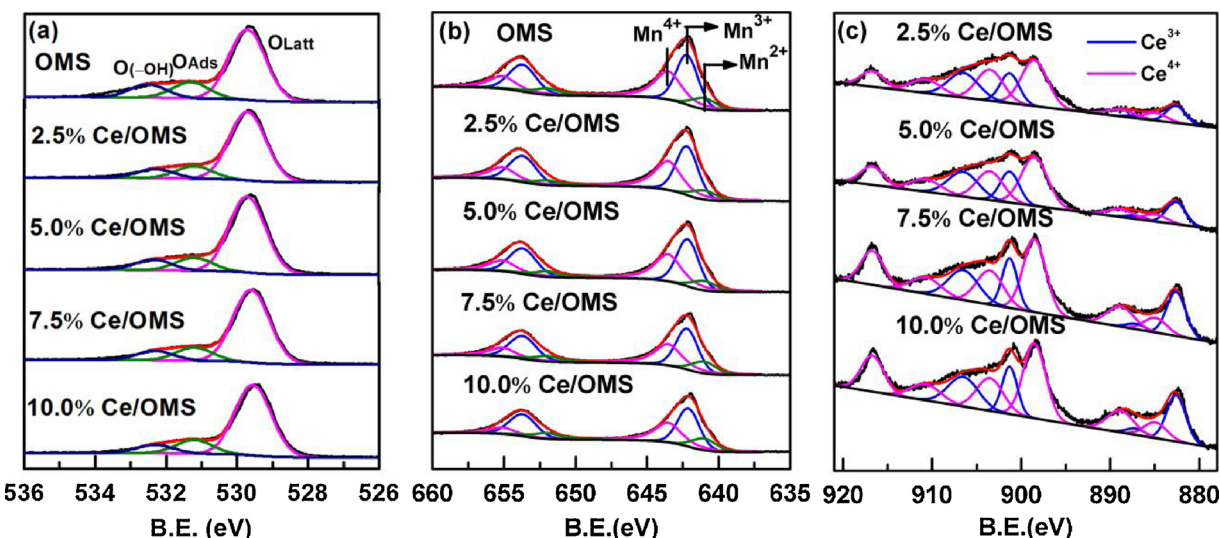
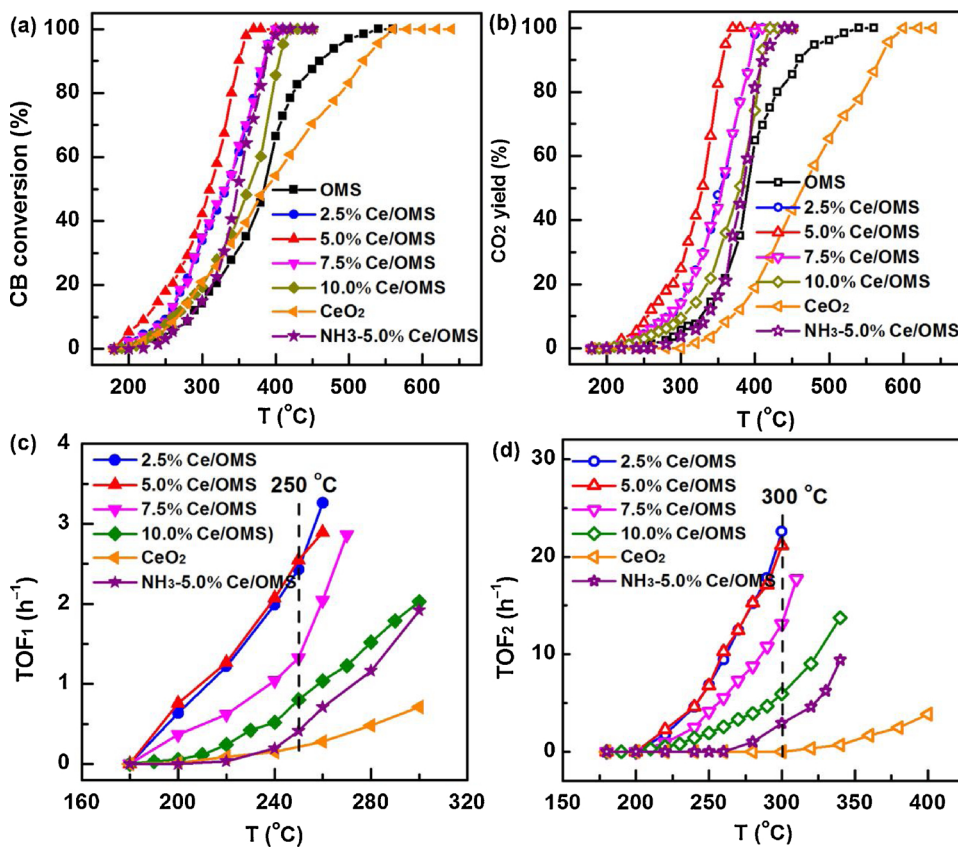


Fig. 5. XPS spectra of various oxides, (a) O-1s, (b) Mn-2p, and (c) Ce-3d orbitals.

Fig. 6. Temperature-dependent performance in catalytic oxidation of chlorobenzene (CB) and the relation of TOF values versus reaction temperature, (a) chlorobenzene conversion, (b) CO<sub>2</sub> yield from chlorobenzene, (c) TOF<sub>1</sub> for chlorobenzene conversion over different catalysts, (d) TOF<sub>2</sub> for CO<sub>2</sub> yield over various catalysts. Reaction condition: WHSV = 60,000 mL/(g h), concentration (CB) = 1000 ppm, and 5 vol.% H<sub>2</sub>O.

reflects the capacity of catalysts to activate pollutant molecule, and the yield of CO<sub>2</sub> as targeted product is considered as capacity to complete mineralization of VOCs. Therefore, we take both VOCs conversion and CO<sub>2</sub> yield into account. From seeing the results in Fig. 6(a and b), CeO<sub>2</sub> is inactive for oxidation of chlorobenzene that the complete degradation requires temperature even above 600 °C, which is ascribed to Cl poisoning active sites [27,33]. It should be noted the demanded temperature for CO<sub>2</sub> yield is higher than that for chlorobenzene conversion, owing to the formation of intermediates such as benzene and maleic acid, which are identified by on-line MS as shown in Fig. S6. These intermediates are easily transformed to carbonic deposit coating catalytic sites, thus demanding to elevate temperature for deep oxidation.

Compared to CeO<sub>2</sub>, the relatively lower temperature is demanded for OMS. The combination of the two oxides via redox etching-precipitation can improve catalytic activity for chlorobenzene oxidation. When 2.5% molar Ce/Mn ratio of CeO<sub>y</sub> is supported on OMS, the temperatures for conversion and mineralization of chlorobenzene are obviously lower than those over CeO<sub>2</sub> and OMS. The increased Ce/Mn molar ratio to 5.0% further reduces reaction temperature. However, when the Ce/Mn molar ratio is raised to 7.5% and 10.0%, the required temperatures turn to higher temperature. In other words, the promotion effect of CeO<sub>y</sub> addition is varied with the change of Ce/Mn molar ratio. The best catalytic activity is reached by 5.0% Ce/OMS. With the same ingredient, the NH<sub>3</sub>-5.0% Ce/OMS catalyst prepared by NH<sub>3</sub>-H<sub>2</sub>O

**Table 4**

The dispersion of Ce species, turnover frequency (TOF) and apparent activation energies for chlorobenzene (CB) conversion and CO<sub>2</sub> yield over different catalysts.<sup>a</sup>

Sample	Ce dispersion (%) <sup>b</sup>	TOF <sub>1</sub> (h <sup>-1</sup> ) <sup>c</sup>	TOF <sub>2</sub> (h <sup>-1</sup> ) <sup>d</sup>	<i>E<sub>a,1</sub></i> of CB conversion (kJ/mol)	<i>E<sub>a,2</sub></i> of CO <sub>2</sub> yield (kJ/mol)
OMS	–	–	–	66.9	115.1
2.5% Ce/OMS	39.2	2.4	22.5	55.4	88.1
5.0% Ce/OMS	41.6	2.5	21.1	46.6	77.7
7.5% Ce/OMS	27.0	1.3	13.1	53.2	81.6
10.0% Ce/OMS	27.3	0.8	5.9	78.2	88.2
CeO <sub>2</sub>	13.6	0.2	0	96.4	108.6
NH <sub>3</sub> -5.0% Ce/OMS	45.0	0.4	2.9	88.5	98.9

<sup>a</sup> Reaction condition: WHSV = 60,000 mL/(g h), concentration(CB) = 1000 ppm, and 5 vol.% H<sub>2</sub>O.

<sup>b</sup> The dispersion of CeO<sub>y</sub> was calculated according to particle size, and the calculation is described in detail in Supporting Information.

<sup>c</sup> The turnover frequency of chlorobenzene per unit of Ce species and reaction time at temperature of 250 °C.

<sup>d</sup> The turnover frequency of CO<sub>2</sub> yield per unit of CeO<sub>2</sub> and reaction time at temperature of 300 °C.

precipitation exhibits a poor performance than 5.0% Ce/OMS.

For a deep insight into the effect of CeO<sub>y</sub> addition onto catalytic performance, the dynamic analysis is studied. As discussion of TEM results, the morphology of CeO<sub>y</sub> supported on OMS is closely related to synthetic method and Ce/Mn molar ratio. According to the particle size measured by TEM, the dispersion values of Ce species are calculated. As listed in Table 4, the Ce dispersion of CeO<sub>2</sub> gives a low value of 13.6% owing to the large particle size. Supporting CeO<sub>y</sub> on OMS reduces particle size of CeO<sub>y</sub>, which causes the increase of Ce dispersion. When Ce/Mn molar ratio is less than 5.0%, the values of Ce dispersion for catalysts prepared by both redox etching-precipitation and NH<sub>3</sub>-H<sub>2</sub>O precipitation are as high as about 40%. When the Ce/Mn molar ratio is higher than 7.5%, the Ce dispersion is decreased to around 27% ascribed to agglomeration of CeO<sub>y</sub> on the surface of OMS. According to dispersion and actual content of Ce, the turnover frequency values of chlorobenzene conversion (TOF<sub>1</sub>) and CO<sub>2</sub> yield (TOF<sub>2</sub>) over unit of Ce species are calculated by controlling 20% of chlorobenzene conversion and CO<sub>2</sub> yield. As depicted in Fig. 6(c–d), the temperature-dependent values of TOF<sub>1</sub> and TOF<sub>2</sub> for 2.5% and 5.0% Ce/OMS are very close and their values are obviously higher than other catalysts at the same temperature as displayed for the values of TOF<sub>1</sub> at 250 °C and TOF<sub>2</sub> at 300 °C. The TOF values of catalysts can be ranked as follow: 5.0% Ce/OMS ≈ 2.5% Ce/OMS > 7.5% Ce/OMS > 10.0% Ce/OMS > NH<sub>3</sub>-5.0% Ce/OMS > CeO<sub>y</sub>, which means 5.0% Ce/OMS and 2.5% Ce/OMS exhibit higher activity of unit Ce species for chlorobenzene oxidation. This phenomenon is probably related to Ce dispersion of catalyst. However, in spite of the similar Ce dispersion and the same ingredient, there is a great difference in TOF values between 5.0% Ce/OMS (TOF<sub>1</sub> = 2.5 h<sup>-1</sup>, TOF<sub>2</sub> = 21.1 h<sup>-1</sup>) and NH<sub>3</sub>-5.0% Ce/OMS (TOF<sub>1</sub> = 0.4 h<sup>-1</sup>, TOF<sub>2</sub> = 2.9 h<sup>-1</sup>). The promotion of catalytic activity for 5.0% Ce/OMS is probably attributed to the strong interfacial interaction between CeO<sub>y</sub> and OMS due to hemi-spheres of CeO<sub>y</sub> lying on support (see TEM analysis) to form Ce-O-Mn bond by chemical etching. The interface effect is thought to provide more active sites for catalytic oxidation of chlorobenzene. Through carefully comparing results for *in-situ* DRIFTS of pyridine adsorption and O<sub>2</sub>-TPD between 5.0% Ce/OMS and NH<sub>3</sub>-5.0% Ce/OMS in Fig. S5, it is clarified that the enhancement of interface effect by redox etching-precipitation facilitates formation of Lewis acid and mobility of lattice oxygen, which is favorable to activation and deep oxidation of chlorobenzene.

Sequentially, the apparent activation energy for chlorobenzene conversion (*E<sub>a,1</sub>*) and mineralization (*E<sub>a,2</sub>*) are calculated by using Arrhenius function ( $K = A \text{Exp}(-E_a/RT)$ ). Notably, chlorobenzene conversion and CO<sub>2</sub> yield are controlled at below 20%. According to chlorobenzene conversion or CO<sub>2</sub> yield at certain temperature and WHSV, reaction rate (r) is calculated, then reaction rate constant ( $K = r/c$ ) is obtained on basis of substrate/product concentration (c) by assuming catalytic oxidation of chlorobenzene as first order reaction at low conversion/mineralization. The Arrhenius plots are linear-fitted as shown in Fig. S7(a and b), and the calculated values of *E<sub>a,1</sub>* and *E<sub>a,2</sub>* are

listed in Table 4. The overall values of *E<sub>a,2</sub>* are higher than *E<sub>a,1</sub>*, namely the complete mineralization of chlorobenzene overcomes higher energy barrier, thus the higher temperature is required for CO<sub>2</sub> yield. The energy barrier can be reduced by supporting CeO<sub>y</sub> on OMS, for instance, the *E<sub>a</sub>* values for 2.5% Ce/OMS (*E<sub>a,1</sub>* = 55.4 kJ/mol, *E<sub>a,2</sub>* = 88.1 kJ/mol) are less than those for individual OMS (*E<sub>a,1</sub>* = 66.9 kJ/mol, *E<sub>a,2</sub>* = 115.1 kJ/mol) and CeO<sub>2</sub> (*E<sub>a,1</sub>* = 96.4 kJ/mol, *E<sub>a,2</sub>* = 108.6 kJ/mol). Because of more active sites at interface, the energy barrier over 5.0% Ce/OMS is further reduced to *E<sub>a,1</sub>* = 46.6 kJ/mol and *E<sub>a,2</sub>* = 77.7 kJ/mol. However, the further increasing of CeO<sub>y</sub> can not improve the physicochemical properties of catalyst. Oppositely, it decreases Ce dispersion and reduces the amount of active sites, therefore, leads to the increasing of *E<sub>a</sub>* values (*E<sub>a,1</sub>* = 53.2 kJ/mol and *E<sub>a,2</sub>* = 81.6 kJ/mol for 7.5% Ce/OMS, *E<sub>a,1</sub>* = 78.2 kJ/mol and *E<sub>a,2</sub>* = 88.2 kJ/mol for 10.0% Ce/OMS). That is, 5.0% Ce/OMS with the appropriate amount of CeO<sub>y</sub> loading possesses the lowest energy barrier and thereby shows the highest catalytic activity. It should be pointed out, despite owning the same molar Ce/Mn ratio, NH<sub>3</sub>-5.0% Ce/OMS has much higher energy barriers than 5.0% Ce/OMS. It could be attributed to weaker interface effect by NH<sub>3</sub>-H<sub>2</sub>O precipitation method, resulting in less improvement in physicochemical properties as shown in Fig. S5.

Since the active sites at interface have a great influence on catalytic performance, the inner principle is researched by combination of structural properties and catalytic performance. As mentioned by characterizations (*in-situ* DRIFTS, NH<sub>3</sub>-TPD, H<sub>2</sub>-TPR, O<sub>2</sub>-TPD and XPS), the appropriate content of CeO<sub>y</sub> loading facilitates enhancement of acidity and lattice oxygen mobility. In general, more acidity and more lattice oxygen at surficial layer are beneficial for oxidation of chlorobenzene. C–X (X = Cl and H) bonds of chlorobenzene can be activated by acidic site, and the lattice oxygen plays a key role to oxidation reaction where MvK mechanism is usually obeyed [7,32,52–54,61]. The improved properties are basically ascribed to the strong interaction between CeO<sub>y</sub> and OMS. The balance of Mn-O-Mn and Ce-O-Ce bond forces at interface is broken by forming Mn–O–Ce bond, where oxygen atom is near to high-valence cation and the electron distribution is varied. As a result, the mobility of lattice oxygen and acidity in superficial layer are affected. The redox etching-precipitation enhances the interfacial interaction and the high dispersion of Ce species can be retained with appropriate Ce/Mn molar ratio. Herein, 5.0% Ce/OMS with optimal ingredient exhibits the best catalytic performance for chlorobenzene oxidation compared to other catalysts. In fact, we have ever reported redox co-precipitation to synthesize Ce-Mn solid solutions for catalytic oxidation of VOCs [25]. Although the interaction between Mn and Ce oxides can be enhanced, a severe issue has to be considered that a lot of active Ce species lost in the bulk of as-prepared material can not take part in oxidation reaction. Therefore, the higher molar ratio (1/5) of Ce/Mn is demanded to satisfy catalytic performance. Even so, its activity is still lower than that of 5.0% Ce/OMS in catalytic oxidation of chlorobenzene.

Given diversity of operation environments in which catalysts work,

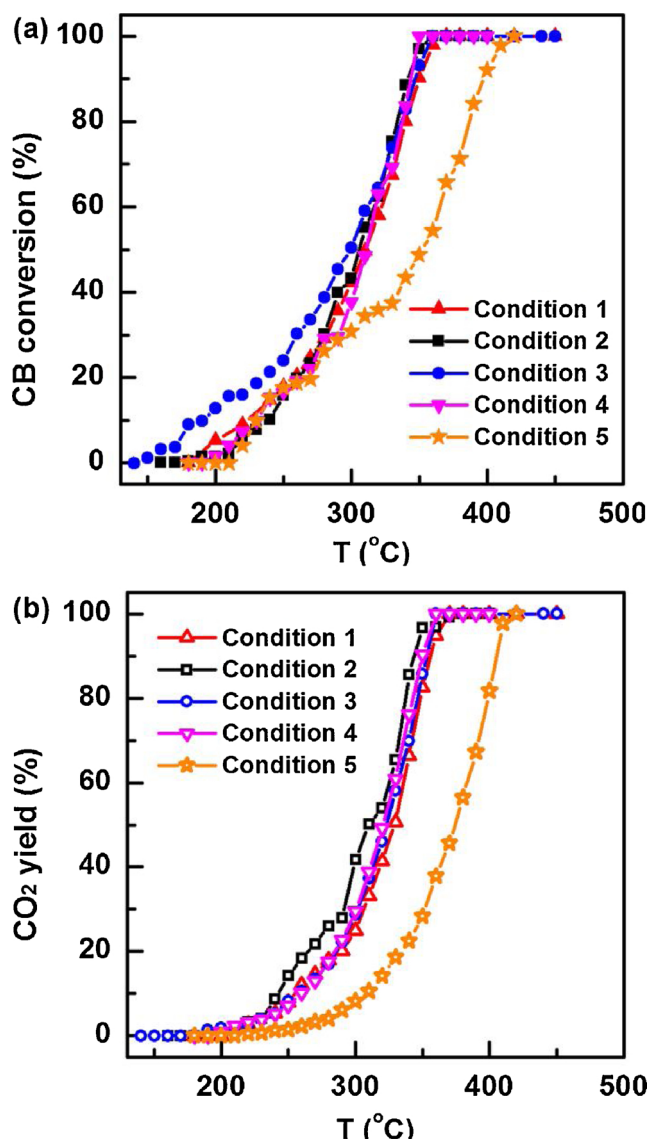


**Fig. 7.** The influence of reaction condition on performance of 5.0% Ce/OMS in catalytic oxidation of chlorobenzene (CB): Condition 1 (concentration = 1000 ppm, WHSV = 60,000 mL/(g h), water content = 5 vol.%); Condition 2 (concentration = 1000 ppm, WHSV = 60,000 mL/(g h), water content = 10 vol.%); Condition 3 (concentration = 1000 ppm, WHSV = 60,000 mL/(g h), water content = 0 vol.%); Condition 4 (concentration = 500 ppm, WHSV = 60,000 mL/(g h), water content = 0 vol.%); Condition 5 (concentration = 1000 ppm, WHSV = 120,000 mL/(g h), water content = 0 vol.%).

it is necessary to investigate the behaviors of catalysts under different conditions such as concentration, weight hourly space velocity (WHSV) and humidity. As depicted in Fig. 7(a and b), over 5.0% Ce/OMS catalyst, only slight changes of catalytic activity are observed when chlorobenzene concentration is varied from 500 ppm to 1000 ppm and water content is controlled in the range of 0–10 vol.%. However, the WHSV has an obvious influence on catalytic removal of chlorobenzene. When the WHSV is increased from 60,000 mL/(g h) to 120,000 mL/(g h), the temperature of chlorobenzene complete degradation is raised from *ca.* 360 °C–410 °C by the reason of shortened retention time of pollutant molecule over catalyst. After the first use for about three months, the spent catalyst of 5.0% Ce/OMS was reused to examine its recycling stability with condition of WHSV = 60,000 mL/(g h), 1000 ppm chlorobenzene and 5 vol.% water. As shown in Fig. 8(a), the catalytic behaviors of spent catalyst at the last three recycles are similar to the first. The XRD result in Fig. 8(b) of the spent catalyst after four

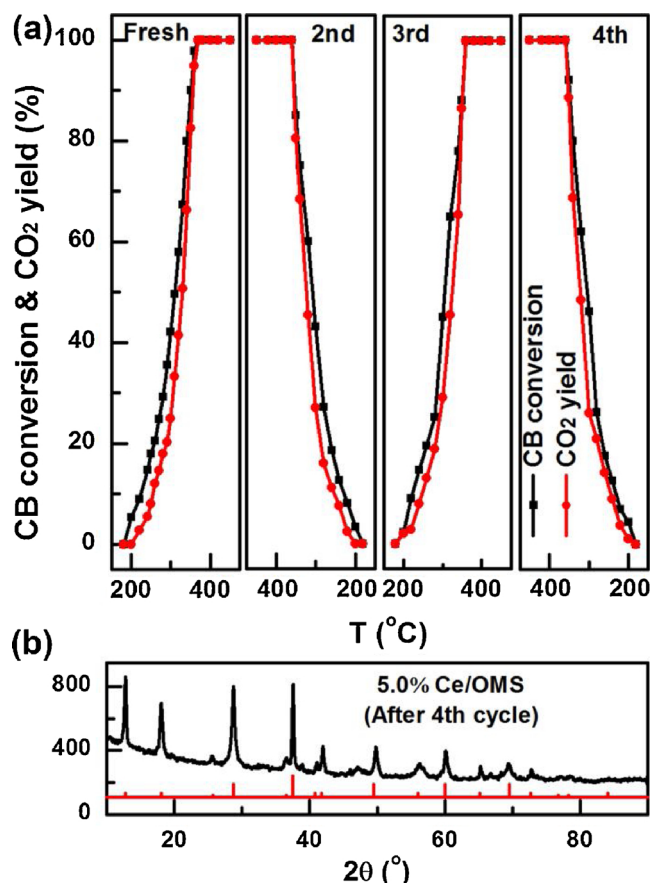


**Fig. 8.** Recycling 5.0% Ce/OMS in catalytic oxidation of chlorobenzene (a) and XRD pattern of spent catalyst after four cycles (b). Reaction condition: chlorobenzene concentration = 1000 ppm, WHSV = 60,000 mL/(g h), water content = 5 vol.%. Notably, the last three cycles were carried out after the first use for about three months.

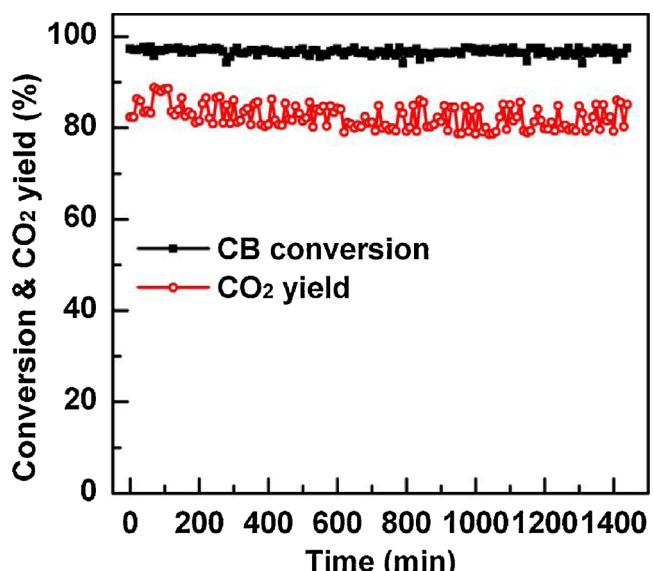


**Fig. 9.** Long-term stability test of 5.0% Ce/OMS catalyst in catalyzing oxidation of chlorobenzene at 350 °C. Reaction condition: chlorobenzene concentration = 1000 ppm, water content = 10 vol.% and WHSV = 60,000 mL/(g h) at 350 °C.

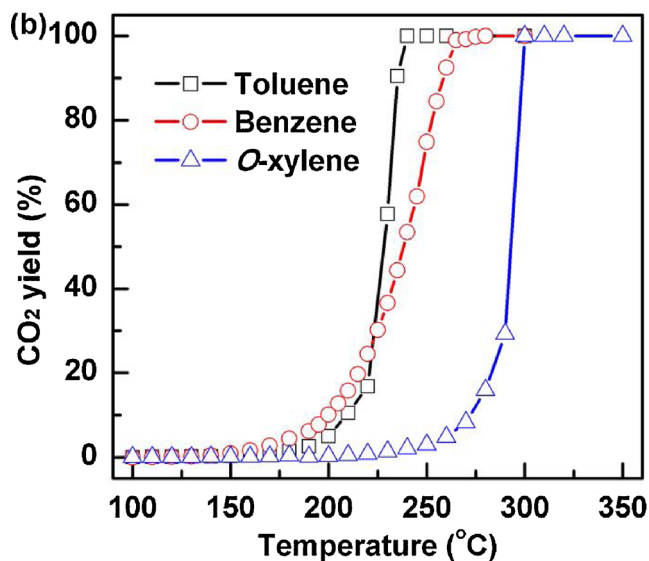
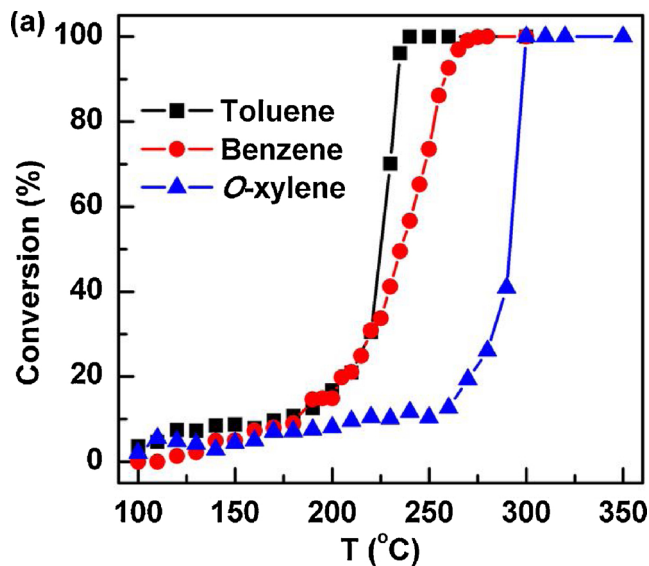


Fig. 10. Catalytic performance of 5.0% Ce/OMS in oxidation of non-chlorinated aromatic VOCs (benzene, toluene and *o*-xylene) into CO<sub>2</sub>, (a) catalytic conversion of non-chlorinated VOCs, and (d) mineralization of non-chlorinated VOCs into CO<sub>2</sub>. Reaction condition: WHSV = 60,000 mL/(g h), concentration (VOCs) = 1000 ppm, and dry air stream.

recycles confirms no obvious change to crystal structure, in other words, the catalyst exhibits a good structural stability. The long-term stability of catalytic performance over 5.0% Ce/OMS has been examined under condition of high humidity (water content = 10 vol.%, 1000 ppm chlorobenzene and WHSV = 60,000 mL/(g h)). As shown in Fig. 9, with reaction temperature of 350 °C, the chlorobenzene conversion and CO<sub>2</sub> yield can remain at around 95% and 85% at least 24 h, respectively. It demonstrates that the as-prepared 5.0% Ce/OMS exhibits good stability at the severe condition.

Considering diversity and complexity of VOCs in industrial off-gas, the investigation of catalytic performance to different VOCs and mixture has been carried out. Three kinds of non-chlorinated aromatic VOCs (benzene, toluene and *o*-xylene, named as BTX) are selected to test the adaptability of 5.0% Ce/OMS in removal of different VOCs. As shown in Fig. 10(a and b), the abilities of complete catalytic degradation of BTX are ranked as order: toluene > benzene > *o*-xylene, where the highest temperature for catalytic removal of BTX is less than 300 °C. Further investigation for catalytic behavior of mixed VOCs has been performed on 5.0% Ce/OMS by using a mixture of 500 ppm

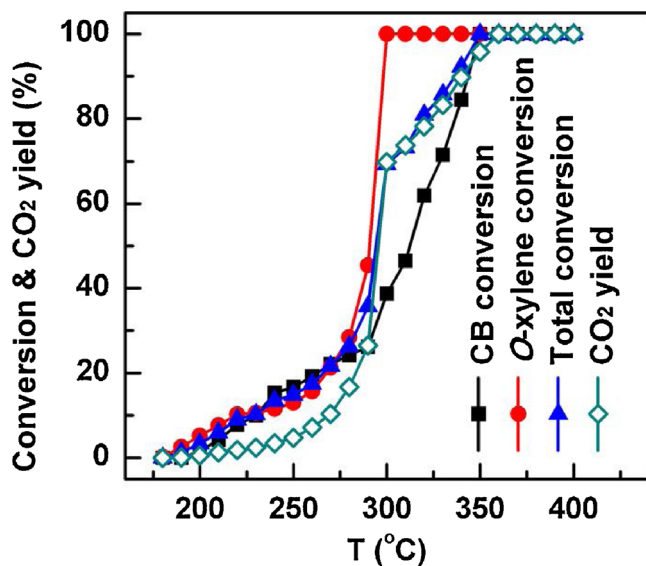


Fig. 11. The performance of 5.0% Ce/OMS in catalytic oxidation of VOCs mixture (chlorobenzene and *o*-xylene). Reaction condition: concentration (chlorobenzene) = concentration (*o*-xylene) = 500 ppm, WHSV = 60,000 mL/(g h) in dry air.

chlorobenzene and 500 ppm *o*-xylene. As observed in Fig. 11, catalytic activity of chlorobenzene oxidation is not affected by mixing *o*-xylene and the temperature for complete oxidation of mixture is about 360 °C.

#### 4. Conclusions

The strategy of redox etching-precipitation is designed for the first time application in synthesis of OMS-supported CeO<sub>y</sub>. As speculated, the hydrolysis of Ce<sup>3+</sup> salt could be driven by consumption of H<sup>+</sup> during redox reaction between MnO<sub>2</sub> and H<sub>2</sub>O<sub>2</sub>. With structure characterizations (TEM, N<sub>2</sub> static physisorption, ICP-OES and XPS), the possibility of this method is evidenced to support stoichiometric amount of CeO<sub>y</sub> on OMS while the surface of OMS is chemically etched to enlarge exposed surface. Compared to conventional method of NH<sub>3</sub>·H<sub>2</sub>O precipitation, the nanostructure of as-prepared metal oxides via our method could improve interfacial contact between CeO<sub>y</sub> and OMS, leading to several changes in physicochemical properties in terms of acidity, oxygen mobility and surface oxygen vacancy. With chemisorption characterization, it is proved that the proper Ce/Mn molar ratio = 0.05 could facilitate formation of more acidity, more surface oxygen vacancy as well as more lattice oxygen in surface. Associated with XPS characterization, these variations are attributed to interfacial effect which is strongly influenced by Ce/Mn molar ratio as well as synthetic method. Generally, the performance is determined by structure. The binary oxides prepared by redox etching-precipitation perform Ce/Mn ratio-dependent activity in catalytic oxidation of chlorobenzene. Among them, 5.0% Ce/OMS with an optimal Ce/Mn molar ratio exhibits the most activity so that the complete removal of 1000 ppm chlorobenzene with WHSV of 60,000 mL/(g h) is achieved at 360 °C. The activity is higher than that of NH<sub>3</sub>-5.0% Ce/OMS catalyst. Associated with characterizations, the close relation between structure and catalytic performance is revealed. In fact, 5.0% Ce/OMS owing more acidity and more active oxygen is competent to activation and oxidation of chlorobenzene. Moreover, the 5.0% Ce/OMS catalyst exhibits good adaptability to different kinds of VOCs, satisfactory tolerance to high content of water and long-term stability at realistic reaction.

## Acknowledgements

This work was supported by National Nature Science Foundation of China [No. 21806162]; “Cooperation of Industry-University-Institute and Scientific and Technological Cooperation” of Xiamen [3502Z20182006]; the “One Hundred Talent Project” from Chinese Academy of Sciences; the “Key Research Program of Frontier Sciences” from Chinese Academy of Sciences [No. QYZDB-SSW-DQC022].

## Appendix A. Supplementary data

Supplementary material related to this article can be found, in the online version, at doi:<https://doi.org/10.1016/j.apcatb.2019.03.042>.

## References

- [1] S.M. Platt, I.E. Haddad, S.M. Pieber, R.J. Huang, A.A. Zardini, M. Clairotte, R. Suarez-Bertoia, P. Barnet, L. Pfaffenberger, R. Wolf, J.G. Slowik, S.J. Fuller, M. Kalberer, R. Chirico, J. Dommen, C. Astorga, R. Zimmermann, N. Marchand, S. Hellebust, B. Temime-Roussel, U. Baltenberger, A.S.H. Prévôt, Two-stroke scooters are a dominant source of air pollution in many cities, *Nat. Commun.* 5 (2014) 3749–3755, <https://doi.org/10.1038/ncomms4749>.
- [2] J.J. Spivey, Complete catalytic oxidation of volatile organics, *Ind. Eng. Chem. Res.* 26 (1987) 2165–2180, <https://doi.org/10.1021/ie00071a001>.
- [3] H.L. Chen, H.M. Lee, S.H. Chen, M.B. Chang, S.J. Yu, S.N. Li, Removal of volatile organic compounds by single-stage and two-stage plasma catalysis systems: a review of the performance enhancement mechanisms, current status, and suitable applications, *Environ. Sci. Technol.* 43 (2009) 2216–2227, <https://doi.org/10.1021/es802679b>.
- [4] K. Everaert, J. Baeyens, Catalytic combustion of volatile organic compounds, *J. Hazard Mater.* 109 (2004) 113–139, <https://doi.org/10.1016/j.jhazmat.2004.03.019>.
- [5] W.B. Li, J.X. Wang, H. Gong, Catalytic combustion of VOCs on non-noble metal catalysts, *Catal. Today* 148 (2009) 81–87, <https://doi.org/10.1016/j.cattod.2009.03.007>.
- [6] B. Puértolas, A. Smith, I. Vázquez, A. Dejoz, A. Moragues, T. Garcia, B. Solsona, The different catalytic behaviour in the propane total oxidation of cobalt and manganese oxides prepared by a wet combustion procedure, *Chem. Eng. J.* 229 (2013) 547–558, <https://doi.org/10.1016/j.cej.2013.06.041>.
- [7] Z. Ren, Z.L. Wu, W.Q. Song, W. Xiao, Y.B. Guo, J. Ding, S.L. Suib, P.X. Gao, Low temperature propane oxidation over  $\text{Co}_3\text{O}_4$  based nano-array catalysts: Ni dopant effect, reaction mechanism and structural stability, *Appl. Catal. B - Environ.* 180 (2016) 150–160, <https://doi.org/10.1016/j.apcatb.2015.04.021>.
- [8] J. Brunet, E. Genty, C. Barroo, F. Cazier, C. Poupin, S. Siffert, D. Thomas, G. De Weireld, T. Visart de Bocarmé, R. Cousin, The  $\text{CoAlCeO}$  mixed oxide: an alternative to palladium-based catalysts for total oxidation of industrial VOCs, *Catalysts* 8 (2018) 64–83, <https://doi.org/10.3390/catal8020064>.
- [9] J. Chen, X. Chen, Z. Xu, W.J. Xu, J.J. Li, H.P. Jia, J. Chen, Syntheses of hierarchical  $\text{MnO}_2$  via  $\text{H}_2\text{O}_2$  selectively reducing  $\text{KMnO}_4$  for catalytic combustion of toluene, *ChemistrySelect* 1 (2016) 4052–4056, <https://doi.org/10.1002/slct.201600921>.
- [10] K. Ramesh, L.W. Chen, F.X. Chen, Y. Liu, Z. Wang, Y.F. Han, Re-investigating the CO oxidation mechanism over unsupported  $\text{MnO}$ ,  $\text{Mn}_2\text{O}_3$  and  $\text{MnO}_2$  catalysts, *Catal. Today* 131 (2008) 477–482, <https://doi.org/10.1016/j.cattod.2007.10.061>.
- [11] S.C. Kim, W.G. Shim, Catalytic combustion of VOCs over a series of manganese oxide catalysts, *Appl. Catal. B - Environ.* 98 (2010) 180–185, <https://doi.org/10.1016/j.apcatb.2010.05.027>.
- [12] W.Z. Si, Y. Wang, S. Zhao, F.Y. Hu, J.H. Li, A facile method for *in situ* preparation of the  $\text{MnO}_2/\text{LaMnO}_3$  catalyst for the removal of toluene, *Environ. Sci. Technol.* 50 (2016) 4572–4578, <https://doi.org/10.1021/acs.est.5b06255>.
- [13] H.W. Du, Y. Wang, H. Arandiyan, A. Younis, J. Scott, B. Qu, T. Wan, X. Lin, J.C. Chen, D.W. Chu, Design and synthesis of  $\text{CeO}_2$  nanowire/ $\text{MnO}_2$  nanosheet heterogeneous structure for enhanced catalytic properties, *Mater. Today Commun.* 11 (2017) 103–111, <https://doi.org/10.1016/j.mtcomm.2017.03.002>.
- [14] P.F. Zhang, H.F. Lu, Y. Zhou, L. Zhang, Z. Wu, S.Z. Yang, H.L. Shi, Q.L. Zhu, Y.F. Chen, S. Dai, Mesoporous  $\text{MnCeO}_x$  solid solutions for low temperature and selective oxidation of hydrocarbons, *Nat. Commun.* 6 (2015) 8446–8455, <https://doi.org/10.1038/ncomms9446>.
- [15] Z.W. Huang, X. Gu, Q.Q. Cao, P.P. Hu, J.M. Hao, J.H. Li, X.F. Tang, Catalytically active single-atom sites fabricated from silver particles, *Angew. Chem. Int. Ed.* 51 (2012) 4198–4203, <https://doi.org/10.1002/anie.201109065>.
- [16] X.F. Tang, Y.G. Li, X.M. Huang, Y.D. Xu, H.Q. Zhu, J.G. Wang, W.J. Shen,  $\text{MnO}_x\text{-CeO}_2$  mixed oxide catalysts for complete oxidation of formaldehyde: effect of preparation method and calcination temperature, *Appl. Catal. B - Environ.* 62 (2006) 265–273, <https://doi.org/10.1016/j.apcatb.2005.08.004>.
- [17] T. Mishra, P. Mohapatra, K.M. Parida, Synthesis, characterisation and catalytic evaluation of iron–manganese mixed oxide pillared clay for VOC decomposition reaction, *Appl. Catal. B - Environ.* 79 (2008) 279–285, <https://doi.org/10.1016/j.apcatb.2007.10.030>.
- [18] H. Wang, C.L. Chen, Y.X. Zhang, L.X. Peng, S. Ma, T. Yang, H.H. Guo, Z.D. Zhang, D.S. Su, J. Zhang, *In-situ* oxidation of carbon-encapsulated cobalt nanocapsules creates highly active cobalt oxide catalysts for hydrocarbon combustion, *Nat. Commun.* 6 (2015) 7181–7186, <https://doi.org/10.1038/ncomms8181>.
- [19] M. Baldi, V.S. Escrivano, J.M.G. Amores, F. Millela, G. Busca, Characterization of manganese and iron oxides as combustion catalysts for propane and propene, *Appl. Catal. B - Environ.* 17 (1998) 175–182, [https://doi.org/10.1016/S0926-3373\(98\)00013-7](https://doi.org/10.1016/S0926-3373(98)00013-7).
- [20] M.R. Morales, B.P. Barbero, L.E. Cadús, Combustion of volatile organic compounds on manganese iron or nickel mixed oxide catalysts, *Appl. Catal. B - Environ.* 74 (2007) 1–10, <https://doi.org/10.1016/j.apcatb.2007.01.008>.
- [21] Y.S. Wu, Y.X. Zhang, M. Liu, Z.C. Ma, Complete catalytic oxidation of *o*-xylene over Mn–Ce oxides prepared using a redox-precipitation method, *Catal. Today* 153 (2010) 170–175, <https://doi.org/10.1016/j.cattod.2010.01.064>.
- [22] D. Delimaris, T. Ioannides, VOC oxidation over  $\text{MnO}_x\text{-CeO}_2$  catalysts prepared by a combustion method, *Appl. Catal. B - Environ.* 84 (2008) 303–312, <https://doi.org/10.1016/j.apcatb.2008.04.006>.
- [23] W.X. Tang, X.F. Wu, G. Liu, S.D. Li, D.Y. Li, W.H. Li, Y.F. Chen, Preparation of hierarchical layer-stacking Mn–Ce composite oxide for catalytic total oxidation of VOCs, *J. Rare Earth* 33 (2015) 62–69, [https://doi.org/10.1016/S1002-0721\(14\)60384-7](https://doi.org/10.1016/S1002-0721(14)60384-7).
- [24] J. Chen, X. Chen, W.J. Xu, Z. Xu, J.Z. Chen, H.P. Jia, J. Chen, Hydrolysis driving redox reaction to synthesize Mn–Fe binary oxides as highly active catalysts for the removal of toluene, *Chem. Eng. J.* 330 (2017) 281–293, <https://doi.org/10.1016/j.cej.2017.07.147>.
- [25] J. Chen, X. Chen, X. Chen, W.J. Xu, Z. Xu, H.P. Jia, J. Chen, Homogeneous introduction of  $\text{CeO}_2$  into  $\text{MnO}_x$ -based catalyst for oxidation of aromatic VOCs, *Appl. Catal. B - Environ.* 224 (2018) 825–835, <https://doi.org/10.1016/j.apcatb.2017.11.036>.
- [26] P. Zhao, Z.S. Lu, S.T. Liu, Manganese-doped  $\text{CeO}_2$  nanocubes for catalytic combustion of chlorobenzene: an experimental and density functional theory study, *J. Nanosci. Nanotechnol.* 18 (2018) 3348–3355, <https://doi.org/10.1166/jnn.2018.14660>.
- [27] H.F. Li, G.Z. Lu, Q.G. Dai, Y.Q. Wang, Y. Guo, Y.L. Guo, Efficient low-temperature catalytic combustion of trichloroethylene over flower-like mesoporous Mn-doped  $\text{CeO}_2$  microspheres, *Appl. Catal. B - Environ.* 102 (2011) 475–483, <https://doi.org/10.1016/j.apcatb.2010.12.029>.
- [28] M. Wu, X.Y. Wang, Q.G. Dai, Y.X. Gu, D. Li, Low temperature catalytic combustion of chlorobenzene over Mn–Ce–O– $\gamma$ - $\text{Al}_2\text{O}_3$  mixed oxides catalyst, *Catal. Today* 158 (2010) 336–342, <https://doi.org/10.1016/j.cattod.2010.04.006>.
- [29] X.Y. Wang, Q. Kang, D. Li, Catalytic combustion of chlorobenzene over  $\text{MnO}_x\text{-CeO}_2$  mixed oxide catalysts, *Appl. Catal. B - Environ.* 86 (2009) 166–175, <https://doi.org/10.1016/j.apcatb.2008.08.009>.
- [30] X.Y. Wang, Q. Kang, D. Li, Low-temperature catalytic combustion of chlorobenzene over  $\text{MnO}_x\text{-CeO}_2$  mixed oxide catalysts, *Catal. Commun.* 9 (2008) 2158–2162, <https://doi.org/10.1016/j.catcom.2008.04.021>.
- [31] J.W. Kan, L. Deng, B. Li, Q. Huang, S.M. Zhu, S.B. Shen, Y.W. Chen, Performance of co-doped Mn–Ce catalysts supported on cordierite for low concentration chlorobenzene oxidation, *Appl. Catal. A - Gen.* 530 (2017) 21–29, <https://doi.org/10.1016/j.apcata.2016.11.013>.
- [32] Z.N. Shi, P. Yang, F. Tao, R.X. Zhou, New insight into the structure of  $\text{CeO}_2\text{-TiO}_2$  mixed oxides and their excellent catalytic performances for 1,2-dichloroethane oxidation, *Chem. Eng. J.* 295 (2016) 99–108, <https://doi.org/10.1016/j.cej.2016.03.032>.
- [33] P. Yang, Z.N. Shi, S.S. Yang, R.X. Zhou, High catalytic performances of  $\text{CeO}_2\text{-CrO}_x$  catalysts for chlorinated VOCs elimination, *Chem. Eng. Sci.* 126 (2015) 361–369, <https://doi.org/10.1016/j.ces.2014.12.051>.
- [34] Q.G. Dai, Z.Y. Zhang, J.R. Yan, Y.J. Wu, G. Johnson, W. Sun, X.Y. Wang, S. Zhang, W.C. Zhan, Phosphate-functionalized  $\text{CeO}_2$  nanosheets for efficient catalytic oxidation of dichloromethane, *Environ. Sci. Technol.* 52 (2018) 13430–13437, <https://doi.org/10.1021/acs.est.8b05002>.
- [35] X.L. Weng, P.F. Sun, Y. Long, Q.J. Meng, Z.B. Wu, Catalytic oxidation of chlorobenzene over  $\text{Mn}_{0.5}\text{Ce}_{1-x}\text{O}_2/\text{HZSM}-5$  catalysts: a study with practical implications, *Environ. Sci. Technol.* 51 (2017) 8057–8066, <https://doi.org/10.1021/acs.est.6b06585>.
- [36] W. Wang, Q. Zhu, Q.G. Dai, X.Y. Wang, Fe doped  $\text{CeO}_2$  nanosheets for catalytic oxidation of 1,2-dichloroethane: effect of preparation method, *Chem. Eng. J.* 307 (2017) 1037–1046, <https://doi.org/10.1016/j.cej.2016.08.137>.
- [37] X. Weng, Q. Meng, J. Liu, W. Jiang, S. Pattisson, Z. Wu, Catalytic oxidation of chlorinated organics over lanthanide perovskites: effects of phosphoric acid etching and water vapor on chlorine desorption behavior, *Environ. Sci. Technol.* 53 (2019) 884–893, <https://doi.org/10.1021/acs.est.8b04582>.
- [38] V.H. Vu, J. Belkouch, A. Ould-Dris, B. Taouk, Removal of hazardous chlorinated VOCs over Mn–Cu mixed oxide based catalyst, *J. Hazard. Mater.* 169 (2009) 758–765, <https://doi.org/10.1016/j.jhazmat.2009.04.010>.
- [39] T.K. Tseng, L. Wang, C.T. Ho, H. Chu, The destruction of dichloroethane over a  $\gamma$ -alumina supported manganese oxide catalyst, *J. Hazard. Mater.* 178 (2010) 1035–1040, <https://doi.org/10.1016/j.jhazmat.2010.02.044>.
- [40] J. Chen, D.X. Yan, Z. Xu, X. Chen, W.J. Xu, H.P. Jia, J. Chen, A novel redox precipitation to synthesize Au-Doped  $\alpha\text{-MnO}_2$  with high dispersion toward low-temperature oxidation of formaldehyde, *Environ. Sci. Technol.* 52 (2018) 4728–4737, <https://doi.org/10.1021/acs.est.7b06039>.
- [41] X. Wang, Y.D. Li, Selected-control hydrothermal synthesis of  $\alpha$ - and  $\beta\text{-MnO}_2$  single crystal nanowires, *J. Am. Chem. Soc.* 124 (2002) 2880–2881, <https://doi.org/10.1021/ja0177105>.
- [42] X. Wang, Y.D. Li, Rational synthesis of  $\alpha\text{-MnO}_2$  single-crystal nanorods, *Chem. Commun.* 7 (2002) 764–765, <https://doi.org/10.1039/B111723H>.
- [43] R.S. Peng, X.B. Sun, S.J. Li, L.M. Chen, M.L. Fu, J.L. Wu, D.Q. Ye, Shape effect of Pt/ $\text{CeO}_2$  catalysts on the catalytic oxidation of toluene, *Chem. Eng. J.* 306 (2016)

- 1234–1246, <https://doi.org/10.1016/j.cej.2016.08.056>.
- [44] C. Liu, H. Xian, Z. Jiang, L.H. Wang, J. Zhang, L.R. Zheng, Y.S. Tan, X.G. Li, Insight into the improvement effect of the Ce doping into the  $\text{SnO}_2$  catalyst for the catalytic combustion of methane, *Appl. Catal. B - Environ.* 176–177 (2015) 542–552, <https://doi.org/10.1016/j.apcatb.2015.04.042>.
- [45] W.J. Ma, Q. Huang, Y. Xu, Y.W. Chen, S.M. Zhu, S.B. Shen, Catalytic combustion of toluene over Fe-Mn mixed oxides supported on cordierite, *Ceram. Int.* 39 (2013) 277–281, <https://doi.org/10.1016/j.ceramint.2012.06.022>.
- [46] F.G. Durán, B.P. Barbero, L.E. Cadús, C. Rojas, M.A. Centeno, J.A. Odrizola, Manganese and iron oxides as combustion catalysts of volatile organic compounds, *Appl. Catal. B - Environ.* 92 (2009) 194–201, <https://doi.org/10.1016/j.apcatb.2009.07.010>.
- [47] B.R. Strohmeier, D.M. Hercules, Surface spectroscopic characterization of manganese/aluminum oxide catalysts, *J. Phys. Chem.* 88 (1984) 4922–4929, <https://doi.org/10.1021/j150665a026>.
- [48] F. Gaillard, P. Artizzu, Y. Brullé, M. Primet, Catalytic combustion of methane: surface characterization of manganese-substituted barium hexa-aluminate catalysts, *Surf. Interface Anal.* 26 (1998) 367–373, [https://doi.org/10.1002/\(SICI\)1096-9918\(19980501\)26:5<367::AID-SIA381>3.0.CO;2-P](https://doi.org/10.1002/(SICI)1096-9918(19980501)26:5<367::AID-SIA381>3.0.CO;2-P).
- [49] G. Blanco, M.A. Cauqui, J.J. Delgado, A. Galtayries, J.A. Pérez-Omil, J.M. Rodríguez-Izquierdo, Preparation and characterization of Ce-Mn-O composites with applications in catalytic wet oxidation processes, *Surf. Interface Anal.* 36 (2004) 752–755, <https://doi.org/10.1002/sia.1755>.
- [50] M.H.M. Ahmed, O. Muraza, A. Galadima, M. Yoshioka, Z.H. Yamani, T. Yokoi, Choreographing boron-aluminum acidity and hierarchical porosity in \*BEA zeolite by in-situ hydrothermal synthesis for a highly selective methanol to propylene catalyst, *Microporous Mesoporous Mater.* 273 (2019) 249–255, <https://doi.org/10.1016/j.micromeso.2018.06.036>.
- [51] B.X. Shen, X.P. Zhang, H.Q. Ma, Y. Yao, T. Liu, A comparative study of Mn/CeO<sub>2</sub>, Mn/ZrO<sub>2</sub> and Mn/Ce-ZrO<sub>2</sub> for low temperature selective catalytic reduction of NO with NH<sub>3</sub> in the presence of SO<sub>2</sub> and H<sub>2</sub>O, *J. Environ. Sci.* 25 (2013) 791–800, [https://doi.org/10.1016/S1001-0742\(12\)60109-0](https://doi.org/10.1016/S1001-0742(12)60109-0).
- [52] H. Huang, C.H. Zhang, L. Wang, G.Q. Li, L. Song, G.C. Li, S.F. Tang, X.B. Li, Promotional effect of HZSM-5 on the catalytic oxidation of toluene over MnO<sub>x</sub>/HZSM-5 catalysts, *Catal. Sci. Technol.* 6 (2016) 4260–4270, <https://doi.org/10.1039/C5CY02011E>.
- [53] F. Bertinchamps, E.M. Gaigneaux, Influence of the reduction state in the bulk and at the surface on the behavior of MoO<sub>3</sub> catalysts in the reaction of 2-butanol (dehydration versus oxidation) in the presence of oxygen, *Catal. Today* 91–92 (2004) 105–110, <https://doi.org/10.1016/j.cattod.2004.03.017>.
- [54] L. Ma, C.Y. Seo, X.Y. Chen, K. Sun, J.W. Schwank, Indium-doped Co<sub>3</sub>O<sub>4</sub> nanorods for catalytic oxidation of CO and C<sub>2</sub>H<sub>6</sub> towards diesel exhaust, *Appl. Catal. B - Environ.* 222 (2018) 44–58, <https://doi.org/10.1016/j.apcatb.2017.10.001>.
- [55] L.F. Liotta, M. Ousmane, G. Di Carlo, G. Pantaleo, G. Deganello, G. Marci, L. Retailleau, A. Giroir Fendler, Total oxidation of propane at low temperature over Co<sub>3</sub>O<sub>4</sub>-CeO<sub>2</sub> mixed oxides: Role of surface oxygen vacancies and bulk oxygen mobility in the catalytic activity, *Appl. Catal. A - Gen.* 347 (2008) 81–88, <https://doi.org/10.1016/j.apcata.2008.05.038>.
- [56] Z. Tian, P.H. Tchoua Ngamou, V. Vannier, K. Kohse Höinghaus, N. Bahlawane, Catalytic oxidation of VOCs over mixed Co-Mn oxides, *Appl. Catal. B - Environ.* 117–118 (2012) 125–134, <https://doi.org/10.1016/j.apcatb.2012.01.013>.
- [57] H. Li, G. Qi, X. Tana, X. Zhang, W. Huang, W. Li, Shen, Low-temperature oxidation of ethanol over a Mn<sub>0.6</sub>Ce<sub>0.4</sub>O<sub>2</sub> mixed oxide, *Appl. Catal. B - Environ.* 103 (2011) 54–61, <https://doi.org/10.1016/j.apcatb.2011.01.008>.
- [58] J.M. López, A.L. Gilbank, T. García, B. Solsona, S. Agouram, L. Torrente-Murciano, The prevalence of surface oxygen vacancies over the mobility of bulk oxygen in nanostructured ceria for the total toluene oxidation, *Appl. Catal. B - Environ.* 174–175 (2015) 403–412, <https://doi.org/10.1016/j.apcatb.2015.03.017>.
- [59] Y. Xu, M.A.A. Schoonen, The absolute energy positions of conduction and valence bands of selected semiconducting minerals, *Am. Mineral.* 85 (2000) 543–556, <https://doi.org/10.2138/am-2000-0416>.
- [60] G.G. Xia, Y.G. Yin, W.S. Willis, J.Y. Wang, S.L. Suib, Efficient stable catalysts for low temperature carbon monoxide oxidation, *J. Catal.* 185 (1999) 91–105, <https://doi.org/10.1006/jcat.1999.2484>.
- [61] L. Nie, D.H. Mei, H.F. Xiong, B. Peng, Z.B. Ren, X.I.P. Hernandez, A. DeLaRiva, M. Wang, M.H. Engelhard, L. Kovarik, A.K. Datye, Y. Wang, Activation of surface lattice oxygen in single-atom Pt/CeO<sub>2</sub> for low-temperature CO oxidation, *Science* 358 (2017) 1419–1423 <http://science.sciencemag.org/content/358/6369/1419>.